Photoexcitation of Si-Si surface states in nanocrystallites

Munir H. Nayfeh, Nikolaos Rigakis, and Zain Yamani
Department of Physics, University of Illinois at Urbana-Champaign, 1110 West Green Street, Urbana, Illinois 61801
(Received 31 January 1997)

Intrinsic localized radiative surface states belonging to Si-Si dimers on the surface of silicon nanocrystallites have been recently predicted. We examine the various photoexcitation pathways involved in populating these molecular states. We include both direct excitation from the ground state and indirect excitation from the photoexcited delocalized excitonic states via quantum tunneling and thermal activation. We determine the absorption and excitation spectra and the quantum efficiency of the photoluminescence as a function of the crystallite size. Our calculation gives a dramatic enhancement in the efficiency for sizes below a critical size of about 1.4 nm. [S0163-1829(97)06528-4]

Radiative surface-related states were suggested[1] to explain the origin of the optical phenomenon in porous silicon,[2–7] but there had been no information about their nature or origin. Recently, the existence of intrinsic localized surface states in silicon nanocrystallites[8] that might behave as luminescent systems has been presented. It was demonstrated, using empirical tight-binding and first-principle local-density calculations, that such states indeed exist under the form of ''self-trapped excitons,'' at Si-Si dimers on the surface of nanocrystallites. Those are stabilized because of the widening of the gap induced by the quantum confinement. It was shown that those states mostly exist on surfaces where the elastic response of the material is the weakest, and for crystallites as small as possible. However, the mechanism for accessing and populating these states remained open.

In this paper, we examine the various photoexcitation pathways involved in accessing and populating these molecular states. We include both direct excitation from the ground state and indirect excitation from the photoexcited delocalized excitonic states via quantum tunneling and thermal activation. We determine absorption and fluorescence spectra and the quantum efficiency of the photoluminescence. Our calculation demonstrates a dramatic enhancement in the efficiency for crystallite sizes below a critical size near 1.4 nm.

Figure 1 gives the partial energy-level diagrams of the surface Si-Si dimer for a crystallite size of 1.03 nm corresponding to 29 silicon atoms. The potential curves were calculated by Allan *et al.* using two different techniques, a total-energy semiemperical tight-binding technique, and a local-density-approximation technique.[8] The diagram gives the potentials of the ground state and the lowest excited state as a function of the dimer interatomic distance. It shows that the ground state has an all-confining single well at the normal tetrahedral interatomic distances (2.35 Å). The excited state has an all-confining double well. The inner well corresponds to a normal nonradiative delocalized excited excitonic state (2.35 Å), while the outer well corresponds to a stabilized radiative trapped excitonic state at the normal next-nearest-neighbor interspacing (3.85 Å).

We calculated the molecular vibrational structure and the absorption, excitation, and fluorescence spectra of the 1.03-nm-crystallite. We divided the procedure into two processes, one for absorption into the outer well via above-barrier excitation and the other for double-well absorption into the inner well of the excited state. These are schematically drawn in Fig. 1. We used a numerical matrix method[9] to determine the vibrational eigenstates and energies of the ground well and the inner and outer wells and the double-well vibrations of the excited state. For the ground state, we

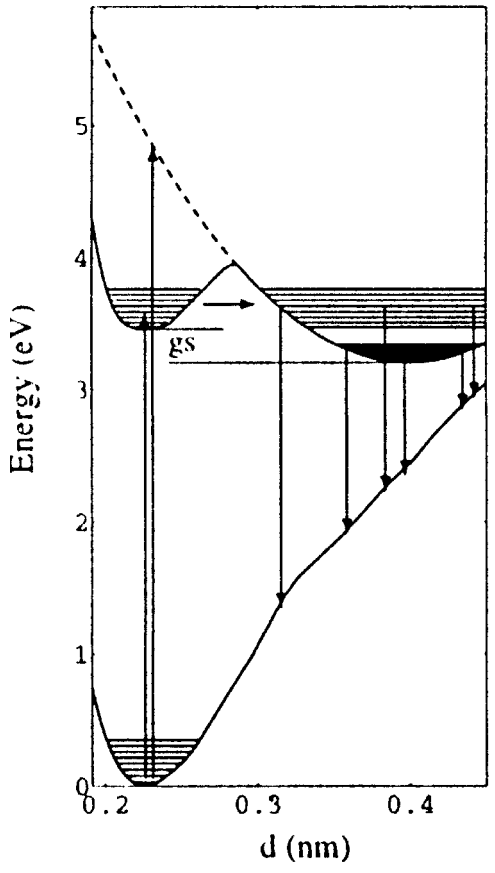

FIG. 1. Partial energy-level diagram of the surface dimers in 1.03-nm crystallite showing the ground and the first excited electronic states. It schematically shows excitation into the inner well via double-well vibrational states, and above barrier excitation into the outer well, along with emission from the double-well states and from the relaxed single outer well.

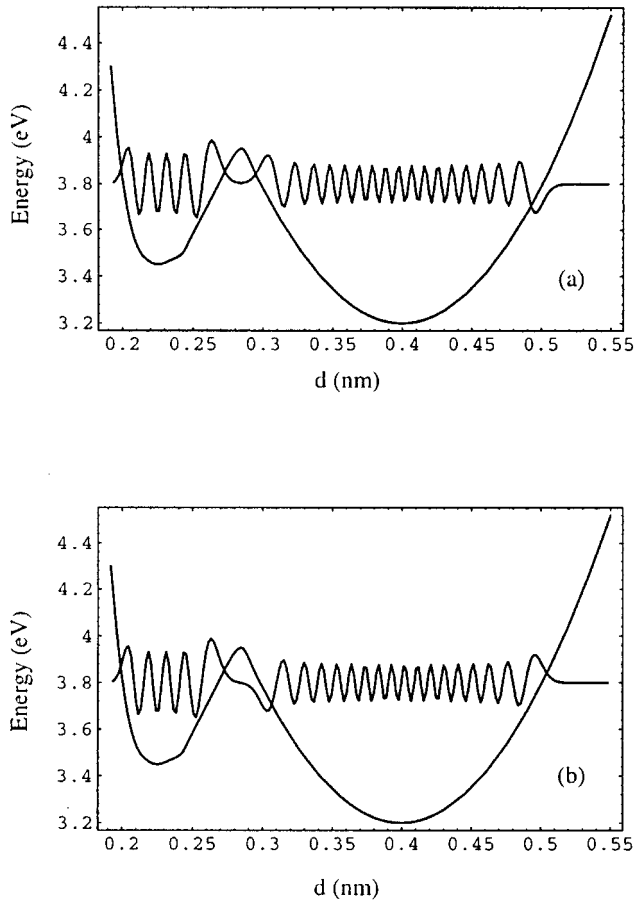

FIG. 2. The double-well vibrational wave function (8,33) in a 1.03-nm crystallite. (a) Bonding and (b) antibonding.

calculated the eigenfunctions and energies in the range $v=0$ to 125, giving, for example, 0.029, 0.078, 0.125, 0.170, 0.215, 0.261, 0.306 eV for the energy of the lowest seven vibrational levels (measured from the bottom of the well). For the outer well of the excited state, we first extrapolated the potential to small and large interatomic distances, and then calculated the eigenfunctions and energies in the range $v=0$ to 150, giving, for example, 3.209, 3.228, 3.247 eV for the lowest three states (measured from the bottom of the ground well). The energy levels of the five lowest vibrational states of the inner well are 3.470, 3.507, 3.545, 3.589, and 3.634 eV.

As a result of tunneling, the system exhibits double-well vibrations in the excited state. Those vibrations were also calculated. Some of the lowest eigenstates (v,v') are (0,14), (1,17), (2,18), (3,21), (4,23), (5,26), (6,28), (7,31), (8,33), (9,35), and (10,37) where v and v' designate the vibrational quantum numbers of the inner and outer wells, respectively. The ground state of this double-well series lies at the bottom of the inner well. We calculated the energies for both the bonding and antibonding wave functions of these states from which one can determine the temporal behavior in the double well. These states can be excited from the $v=0$ ground state at photon excitation energy of 3.440, 3.477, 3.516, 3.560, 3.605, 3.649, and 3.691 eV, respectively. For example, Fig. 2 shows the (8,33) bonding and antibonding double-well states. The energy splitting of the states is 9.84×10^{-6} eV, which gives 0.2 ns for the oscillation period between the two constituent wells.

According to the Franck-Condon principle, the most probable transition in absorption is that proceeding vertically up from the minimum of the lower potential curve. The Einstein electronic transition probability in absorption B, takes the form

$$B=\frac{2\pi^2}{3n^2\varepsilon_0 h^2}\,|\overline{R_e}|^2\left|\int \Psi_{v'}^{*}\Psi_v d\mathbf{r}\right|^2,$$

where $|\overline{R_e}|^2$ is the square of the average electronic transition matrix element, $\psi_{v'}$ and ψ_v are the vibrational eigenfunctions of the upper and lower states, and n is the refractive index. We calculated the absorption probability up to 6 eV. We divided the procedure into two processes, one for absorption into the outer well and the other for double-well absorption into the inner well of the excited state. For excitation into the outer well, Fig. 1 shows that the minimum of the upper state lies at a much larger interatomic separation (4 Å) than that of the ground state (2.35 Å). Thus, according to the Franck-Condon principle, transition from minimum to minimum is not possible. Direct excitation into the outer well must, therefore, proceed vertically from the bottom of the well of the ground state (at $R=2.35$ Å) to the upper excited vibrational states at the same R (see the extrapolation of the potential curve of the outer well). This excitation process, shown schematically in Fig. 1, proceeds at energies around 4.93 eV, that is, at energies above the top of the barrier. For instance, the transition at 4.93 eV corresponds to excitation from the $v=0$ in the ground well to $v=110$ in the extrapolated outer well. For this case, the overlap maximizes with the square of the overlap integral being 0.043. It is for this vibrational level that we have the left turning point lie in the neighborhood of $R=2.35$ Å, the peak position of the ground $v=0$ state. Other upper vibrational states contribute since the extrapolated upper potential is steep and the wave function of $v=0$ ground state has a spread of about 0.2 Å. Excitation of the system can also proceed from the $v=1$ ground state to high-lying levels. Because the maxima of the wave function of $v=1$ state lie near the turning points, we expect appreciable excitation to proceed near the two interatomic separations corresponding to the two turning points. For instance, for photon excitation at 4.73 eV, the vibrational overlap maximizes to a value of 0.031 for $v=98$. On the other hand, for excitation at 5.05 eV, the vibrational overlap maximizes to 0.031 for $v=124$. Other upper vibrational states also contribute but to a lesser degree.

Let us now consider the double-well excitation to the normal delocalized excited excitonic state, i.e., into the inner well of the excited state. The minimum of the upper well occurs at 2.35 Å; thus it lines up with the minimum of the ground-state well. Moreover, the widths of the two wells compare well. Thus, the low-lying levels of the two are similar. Differences due to the anharmonicity are important for levels with $v>5$. Therefore, the most probable excitation is from $v=0$ of the ground well to the lowest double-well state (0,14) at a resonance photon energy of 3.44 eV. The square of the vibrational overlap for this channel is 0.99. The rest of the excitations from $v=0$ of the ground well to all of the upper double-well vibrational levels combined add only to 0.01, as expected from sum rules. Because the upper and lower wells have nearly identical low-lying structure, then

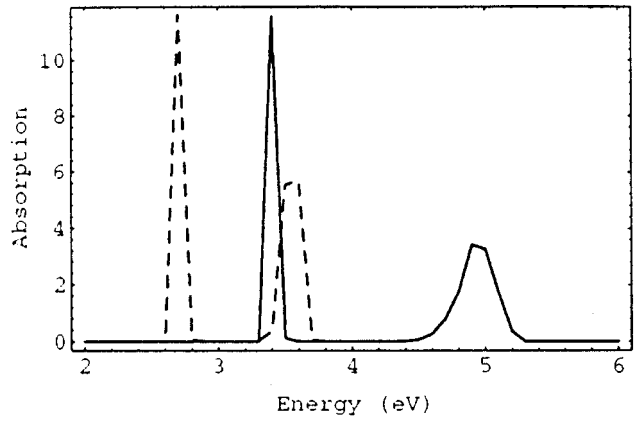

FIG. 3. The transition probability in absorption for photon excitation in the range 0–6 eV (solid) for the 1.03-nm and (dashed) for the 1.67-nm crystalites.

for photon energy of 3.44 eV, resonance excitation commences from the excited states of the ground well. For instance, the square of the overlap integrals from $v=1$ to the $v=0$, 1, 2, and 3 of the upper state are 0.000 07, 0.972, 0.010, and 0.016. Thus the contribution of the 1-1 transition is the dominating one. Similarly excitation from $v=2$ will be dominated by the 2-2 transition with a contribution of 0.959. Averaging over the thermal population of the ground state gives nearly an overlap of unity. This effectively means that most of the population of the ground state is available for excitation to the upper inner well at near unity overlap integral.

Figure 3 gives the results for the transition probability in absorption as function of the excitation photon energy up to 6 eV. The spectrum exhibits a strong sharp isolated peak at 3.44 eV in addition to a wider but weaker peak in the range 4.7–5.2 eV. The sharp peak results from double-well excitation into the inner well. The wide peak is actually composed of three overlapping progressions of peaks, effectively producing a near continuum. They are a result of above the barrier excitation directly into the outer well. We plotted the envelope of the sum of the progressions instead of their individual vibrational states to avoid confusion. The absorption probability was thermally averaged with $T=300$ K.

We performed similar calculations for a larger crystallite. Figure 4 shows the energy-level diagram of the dimer in a crystallite of 1.67 nm corresponding to 123 atoms. The potential curves were calculated by Allan *et al.*[8] For this size, the double-well states (v,v') are found to be (6,0), (7,4), (8,8), (9,12), and (10,16) where v and v' designate the vibrational quantum numbers of the inner and outer wells, respectively. It is to be noted that, unlike the case of the 1.03-nm crystallite, the ground state of the double-well series lies at the bottom of the outer well, considerably above the bottom of the inner well. For each state, we calculated the splitting of the bonding and antibonding wave functions. The first five double well states can be excited from the $v=0$ ground state at photon excitation energy of 2.973, 3.014, 3.055, 3.096, and 3.137 eV, respectively. For example, Fig. 5 shows the (10,16) bonding and antibonding double-well states. The energy difference of the states is 1.0×10^{-5} eV, which gives 0.2 ns for the oscillation period between the two

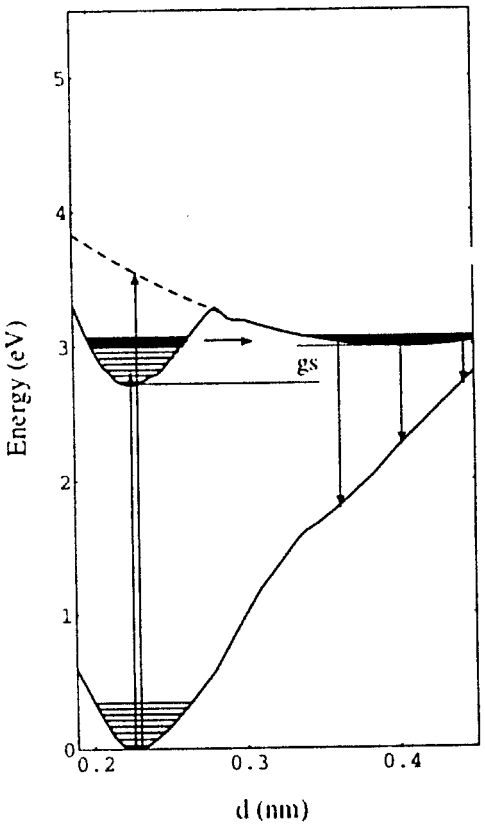

FIG. 4. Partial energy-level diagram of the surface dimers in 1.67-nm crystallite showing the ground and the first excited electronic states. It shows excitation into the inner well and above-barrier excitation into the outer well, along with emission from the double-well states and from the relaxed single outer well.

constituent wells. But these states do not lie at the bottom of the inner well, and therefore cannot be excited strongly from the vibrational ground state of the ground-state well. Strong excitation proceeds to the $v=0$ and 1 in the bottom of the single inner well of the excited state. The results of the calculation for the absorption as a function of the photon energy of the excitation in the energy range up to 6 eV are presented above in Fig. 3 for convenient comparison with those for the 1.03-nm size. The spectrum shows a single large sharp peak at 2.67 eV due to absorption into the inner well, in addition to three overlapping weaker progressions of peaks in the range 3.38–3.61 eV that effectively produce a near continuum. The progressions are a result of excitation above the barrier directly into the outer well. Thus, compared to the results of the small crystallite, the spectrum as a whole exhibits a redshift. In addition, there is an increase in the peak height and narrowing of the width of the continuum peak.

The photoluminescence activity of the system is governed by both the outer and inner wells. Thus to investigate the emission and the quantum efficiency, we determine the overall population in the individual wells. For this, we determine the coupling between the two wells. The two are coupled by temperature activation and by quantum-mechanical tunneling effects (double-well oscillations). We will first consider excitation into the inner well. Let us consider now the single-well vibrations. For two wells of fractional populations N_1 and N_2, thermal equilibrium at temperature T is achieved when $N_1\gamma_1=N_2\gamma_2$ where $\gamma=fe^{-(V-E)/kT}$, E is the energy

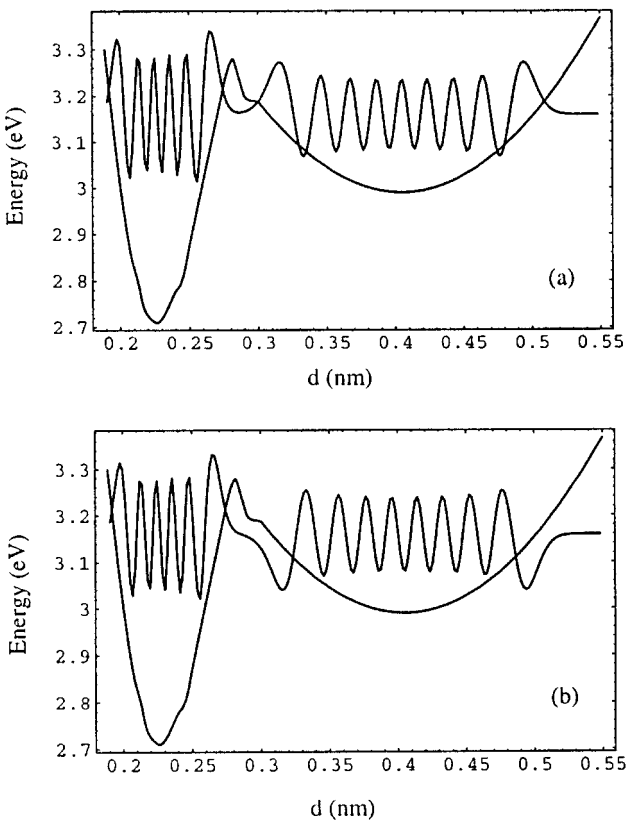

FIG. 5. The double-well vibrational wave function (10,16) in a 1.67-nm crystallite. (a) Bonding and (b) antibonding.

of the ground vibrational state, f is the frequency of oscillation, and V is the barrier height. The equilibrium fractional populations resulting from thermalization are given by the following transfer function:

$$N_2=(f_1/f_2)e^{-g_S/kT}/[1+(f_1/f_2)e^{-g_S/kT}]$$

where $g_S=V_{m2}-V_{m1}$ is the energy difference of the vibrational ground states of the upper wells or, for nearly comparable wells, is the difference between the bottom of the two wells (the gap between the two wells), f_1 and f_2 are the vibrational frequencies in the wells, and $N_1=1-N_2$. For cystallite size of 1.03 nm where $g_S=-0.25$ eV, and $f_1/f_2=2$, N_2 is found to be nearly unity ($N_1\sim 4.5\times 10^{-5}$). Therefore, thermalization of the two single wells results in the total population being effectively in the outer well, i.e., the population of the inner well has been completely transferred to the outer well.

The duration needed for the thermal transfer from the inner well to the outer well via a certain level of energy E is determined from its activation rate and the thermal population. The thermal activation from the various vibrational levels of the inner well to the outer well is calculated to be 2.5, 0.438, and 0.081 μs for the lowest three levels $v=0$, 1, and 2, respectively. The next levels, $v=3$, 4, 5, and 6, fall in the nanosecond regime: 13, 2.2, 0.39, and 0.07 ns, respectively.

As to the double-well vibrations, tunneling (in the 1.03 nm size), the population will exhibit oscillations between the two wells. The period of the oscillation, calculated from the splitting of the bonding and antibonding states, is found to be 700 s, 7 s, 69 ms, 0.74 ms, 30 μs, 0.7 μs, 0.041 μs, 2.03 ns, 0.21 ns, 0.0164 ns, and 0.002 77 ns.

As to the 1.67-nm size where $g_S=0.27$ eV, and $f_1/f_2=4$, N_1 is found to be nearly unity ($N_2\sim 10^{-5}$); that is, the radiating states in the outer well are nearly empty. This shows a large enhancement in the population efficiency of the smaller crystallites over the larger ones when excited in the inner well.

Let us now consider above barrier excitation directly into the outer well. In the case of the 1.03-nm crystallite, the strength of the above barrier excitation is ~ 0.33 of the inner well excitation as seen in Fig. 3. The high-lying vibrational levels will relax into the bottom of the outer well and the double-well states. Since the double-well vibrations lie at higher energy than the single-well vibrations we expect some branching ratio into those vibrations. Those cascading into the bottom of the well will stay frozen. The double-well vibrations will oscillate between the two wells. Thus, most of the population will be available for emission from the outer well.

For the 1.67-nm crystallite, the strength of the above barrier excitation is ~ 0.54 of the inner-well excitation as seen in Fig. 3. The high-lying vibrational levels will relax into the single- and double-well vibrations of the outer well. In this crystallite, both the single-well and double-well vibrations lie at the bottom of the well which might drastically reduce the double-well branching ratio in favor of single-well vibrations. Those cascading into the single outer-well vibrations will be unstable and will be thermalized into the inner well since the inner is the most stable of the two. The time duration for thermal activation for the (6,0), (7,4), (8,8), (9,12) (10,16), and (11,20) double-well states are found to be 3.6 ns, 0.73 ns, 0.144 ns, 29 ps, 6.5 ps, and 1.46 ps, respectively. However, the double-well vibration which, here, lies near the bottom of the well, allows some of the population from the direct excitation to oscillate between the two wells, preventing thermalization into the bottom of the inner well where they become inaccessible for radiative emission. The tunneling time for those states is found to be 99 ms, 2.04 ms, 2.59 μs, 13.6 ns, 0.207 ns, and 0.003 ns, respectively. The ratio of the thermal population in the inner and outer wells due to double-well vibrations converges to a value of 4.0, the ratio of vibration frequency in the two wells. Thus, weak but larger population than what is expected from thermalization alone results from the direct excitation.

Since experimental conditions may involve a distribution of crystallite sizes, it is interesting to discuss other crystallite sizes. First the absorption is expected to be dominated by excitation in the inner well. But the most drastic difference in the efficiency of population of the outer well between large and small crystallites is a direct outcome of the relative position of the minimum of the inner and outer wells, governed by g_S the stability gap. Since we expect g_S to vary with size, we examine N_2 as a function of g_S for both g_S larger than zero and less than zero (i.e., as a function of size). For large crystallites, the inner well lies below the outer one ($g_S>0$), thus its population is stable against that of the outer well. Thermalization tends to transfer the population from the outer well and freeze nearly all of the combined population into the inner one whether the excitation was achieved directly in the inner well or into the outer well. However, it

is not a complete runaway condition. Double-well vibrations resulting from tunneling between the outer and inner wells, if excited during the relaxation, would keep some population oscillating between the two wells. This fraction of the population will then be available for emission from the outer well. As the size is decreased below 1.67 nm, both wells rise to higher energies due to the confinement effects; the inner well rises faster than the outer well, and thus the gap between the well minima will decrease. At a certain size, the inner well catches up with the outer one and g_S vanishes. At this critical size, the ground state of the double-well series lie at the bottom of both wells, and the quantum-mechanical tunneling channel opens up from the inner to the outer well. Intermediate size crystallite potentials are not currently available, so we cannot determine the exact critical size. However, we conjecture that it is for a crystallite with the number of surface and bulk atoms nearly equal. From fcc crystal structure and the result for the 29 atom crystallite[8] we project that the stability gap becomes zero in the range 70 to 60 atoms corresponding to a diameter of about 1.4 nm.[10] This remains to be tested by accurate calculations. For further size reduction, the stability gap becomes negative and grows in magnitude and the outer well becomes the most stable of the two. Thus, the transfer from inner to outer continues to build up strength with the size reduction, eventually attaining an efficiency of unity. At the critical size, the nature of the material changes dramatically. The material becomes highly active optically with an enhancement of several orders of magnitude. It is as if the material has changed from an indirect-gap to a somewhat direct-gap material. We should mention here that other interesting effects have been predicted recently when the size of crystallite drops below critical sizes. Based on symmetry, below a critical size, indirect semiconductors become less indirect and direct ones may become indirect.[11]

The Einstein transition probability in emission A and therefore, the emitted intensity can be obtained from the expression

$$A=\frac{16\pi^3\nu^3 n}{3h\varepsilon_0 c^3}\,|\overline{R_e}|^2\left|\int \Psi_{v'}^{*}\Psi_v d\mathbf{r}\right|^2,$$

where ν is the frequency of the emitted photon. The intensity of the spectral line in emission $I_{\mathrm{em}}=NA\,h\nu$ where N is the number of emitting states. The overlap integrals are evaluated for transition between the vibrational levels of the outer well v' and the vibrational levels of the ground well v. Emission commences from both the states of the double well and from the states of the outer well. For the 1.03-nm crystallite, the states of the double-well initially populated are (0,14) and (1,17). These are the lowest states. Thermalization of the double-well results in some migration of the population to even higher states. Thermal and nonlinear processes may also decouple the system whereby the system begins to oscillate at the single-well vibrations. In this case, thermalization will bring the population of the vibrational levels of the excited molecules of the double-well regions to the region near the band edges (bottom of the outer well) in a time scale of 1 ps.

Thus, we expect emission from the thermal double-well distribution and from the thermal single outer-well distribution. The branching ratio may depend on the origin of the population, direct or through the inner well, and on mixing processes. Figure 6 gives the emission as a function of energy of the emitted photons for the 1.03 nm crystallite for excitation in the double-well vibrations at 3.4 eV. We used 90:10 branching ratio for the double-well to single-well contribution for illustration. The low-energy band emanates from the thermal distribution of the single outer well and extends from 0.5 to 1.5 eV. The higher-energy band extends from 0.8 to 2.2 eV. It corresponds to emission from high-lying double-well states at the left turning point. Emission at the right turning points is expected to be extremely weak. The corresponding results of the 1.67-nm-size crystal are shown in Fig. 6 for excitation in the outer well at 3.5 eV (excitation in the inner well does not contribute). Again we used 90:10 for the branching ratio. First we note, that the 1.67-nm crystallite has a drastically lower intensity compared to that from the 1.03-nm crystallite. We normalized the otherwise weaker emission from the 1.67-nm crystallite to that of the 1.03-nm crystallite, because the absolute emission depends on unknown cascading branching ratio. Second, the double-well and the single-well emission bands overlap because the outer well lies at higher energy than the inner one. The emission extends from 0.4 to 1.8 eV. Thus, the emission widens from a range of 0.4–1.8 eV in the larger crystal to the range of 0.5–2.2 eV for the smaller one, and exhibits a blueshift of 0.4 eV.

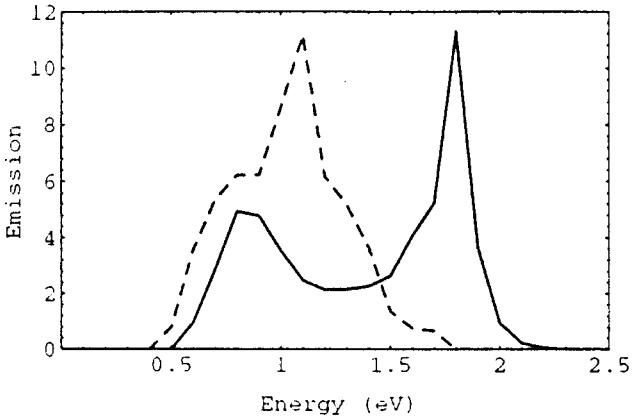

FIG. 6. Normalized emission spectra (solid) from a 1.03-nm crystallite excited in the double-well vibrations at photon energy of 3.5 eV, and (dashed) the otherwise much weaker from a 1.67-nm crystallite for above the barrier excitation at photon energy of 3.5 eV. The high-lying vibrational levels will relax into the bottom of the outer well and the double-well states.

It is to be noted that the first excited electronic state is the only state known for these dimers at this time. It would be interesting to calculate the potential curves of the higher-lying states. Excitation to such states using single photon excitation is expected to be in the vacuum ultraviolet. Excitation, however, can proceed at lower wavelengths via higher-order radiative processes: multiphoton or multistep excitation using high-intensity laser radiation. Direct emission from those states would be beyond the acceptance of visible radiation detectors. However, cascading processes to the lowest excited state would contribute to the visible/IR signals. Therefore, in the absence of such information on the high-lying excited states, the validity of this calculation is restricted to photon energy less than 6 eV and to lower in-

tensity. As to the vibrational structure, we used excitation to a single vibrational level, but in an experiment with radiation of finite bandwidth, several levels might be simultaneously excited. However, at room temperature, thermal effects would mix the levels on a picosecond time scale, much faster than the transfer time between the wells and the emission lifetime. Thus for excitation using lamps or using continuous wave coherent laser radiation, the contribution of the various excited vibrational levels can be incoherently summed over. At lower temperatures, or when examining short-time processes on the subpicosecond regime, the treatment must be modified if several levels are coherently excited.

Finally, these results can be used to generate spectra for real experimental situations. Experimental spectra involve distributions of crystallite sizes. In this case, one needs to calculate all the potential curves for all sizes available in the distribution followed by calculations of the transition probabilities, application of the transfer function, integration over the excitation bandwidth, and sum over the size distribution to yield excitation and fluorescence spectra for comparison with experiment.

In conclusion, we calculated the various photoexcitation pathways involved in populating the molecular states. We included both direct excitation from the ground state and indirect excitation from the photoexcited delocalized excitonic states via quantum tunneling and thermal activation. We determined the absorption and emission spectra and the quantum efficiency of the photoluminescence in crystallites of sizes less than 2 nm. Our calculation gives a dramatic enhancement in the efficiency for sizes below about 1.4 nm. It is as if the material has changed from an indirect-gap to a direct-gap material. Most experiments dealing with effects in crystallites have so far used sizes in the range of 2–4 nm, outside the range considered here.

[1] F. Koch, V. Petrova-Koch, and T. Muschik, J. Lumin. **57**, 271 (1993).

[2] L. T. Canham, Appl. Phys. Lett. **57**, 1046 (1990).

[3] J. P. Proot, C. Delerue, and G. Allan, Appl. Phys. Lett. **61**, 1948 (1992); C. Delerue, G. Allan, and M. Lannoo, Phys. Rev. B **48**, 11024 (1993).

[4] J. C. Vial, A. Bsiesy, F. Gaspard, R. Herino, M. Ligion, F. Muller, R. Romestain, and R. M. Macfarlane, Phys. Rev. B **45**, 14 171 (1992).

[5] P. D. J. Calcott, K. J. Nash, L. T. Canham, M. J. Kane, and D. Brumhead, J. Phys., Condens. Matter. **5**, L91 (1993).

[6] S. Schuppler, S. L. Friedman, M. A. Marcus, D. L. Adler, Y. H. Xie, F. M. Ross, T. D. Harris, W. L. Brown, V. J. Chabal, L. E. Brus, and P. H. Citrin, Phys. Rev. Lett. **72**, 2648 (1994).

[7] D. J. Lockwood, Solid State Commun. **92**, 101 (1994).

[8] G. Allan, C. Delerue, and M. Lannoo, Phys. Rev. Lett. **76**, 2961 (1996).

[9] William R. Gibbs, *Computation in Modern Physics* (World Scientific, Singapore, 1994), p. 149.

[10] Z. Yamani, N. Rigakis, and M. Nayfeh (unpublished).

[11] Shang Yuan Ren (private communication).